

Geometric quantum gates via dark paths in Rydberg atoms

Zhu-yao Jin¹ and Jun Jing^{1,*}

¹*School of Physics, Zhejiang University, Hangzhou 310027, Zhejiang, China*

(Dated: July 17, 2023)

Nonadiabatic holonomic quantum computation provided a promising method to construct high-speed geometric quantum gates. It is featured with a near-perfect resilience to external noises, yet is found to be susceptible to systematic errors. The latter could be partially relieved by the dark-path scheme in the closed-system scenario. Based on an effective four-level configuration, we here construct a universal set of nonadiabatic holonomic controlled gates via dark paths in Rydberg atoms. Distinct from the existing dark-path scheme, our gates can be conveniently realized and manipulated by the off-resonant driving fields on both control atom and target atom. The driving on the control atom can enhance significantly the robustness of the quantum gates against systematic errors while maintaining the resilience to external noises. Our scheme can be straightforwardly generalized to the N -qubit situation. And the three-qubit gate is less susceptible to errors than the double-qubit one.

I. INTRODUCTION

Quantum computation is believed to be more powerful than classical computation in solving certain NP-hard problems, such as factoring larger integers [1] and searching over unsorted databases [2]. Controlled gates are essential elements in the circuit-based quantum computer, which have been widely used in quantum error correction [3, 4] and quantum algorithm [5–8]. In comparison to the quantum circuit composed of many one-qubit gates [9] and two-qubit gates [9–12], the utilization of N -qubit controlled gates [9, 11–13] can reduce the number of quantum gates and then lead to more convenient and higher speed quantum information processing.

Many efforts were made to construct controlled gates in several physical platforms, such as trapped ions [14–16], superconducting circuits [17–19], linear optics [20–22], and neutral atoms [23–31]. Among them, the neutral atoms manifest distinguishable advantages on a long lifetime and a strong Rydberg-Rydberg interaction (RRI), i.e., the dipole-dipole or van der Waals interaction between the high-lying Rydberg states. By virtue of RRI, the neutral atoms demonstrate two opposite phenomena in dynamics which are useful in quantum control: (i) the Rydberg blockade [32–34] that once an atom is excited to the Rydberg state, then the other atoms within the blocking radius will be inhibited from being excited, and (ii) the Rydberg antiblockade [35–38] in which the RRI is compensated by the detuning of laser fields, and then more than one atom can be excited. Though two- and multi-qubit gates based on RRI have been realized in experiments [23, 39–43], the high-fidelity gates are still under the challenge of the inevitable environmental noises and systematic errors.

Noise-resilient quantum gates [44–47] can be generated using the geometric phase [48–51] that depends on the global properties rather than the local details

on the adiabatic evolution path. The adiabatic geometric gates [52–54] based on either Abelian [49] or non-Abelian [48] phases, however, require an adiabatic evolution. Considerable errors will be otherwise accumulated and then give rise to undesired transition and decoherence. Diabatic (fast) evolution could be realized by nonadiabatic holonomic quantum computation (NHQC) [55]. It was further improved by using the decoherence-free subspace [56], the single-shot-shaped pulses [57], a single-loop path [58], and the dynamical decoupling technique [59, 60]. In the NHQC variants that have been experimentally implemented [61–65], the geometric gates are found to be sensitive to the systematic errors [66, 67] arising out of the imperfect state preparation and operation [68, 69]. To overcome this weakness, nonadiabatic holonomic quantum computation with two dark paths (NHQCTD) [70, 71] has been proposed by virtue of the dressed-state technique [72]. Both single-qubit [70] and single-qutrit logic gates [71] of the dark-path schemes in the trapped-ion systems are constructed with an ancillary system. In the ideal situation of the closed system, the dark-path schemes have a complete advantage over the standard NHQC method in resistance to the global error in Rabi-frequency. In the presence of the external decoherence, the NHQCTD scheme yields however a poorer performance than the NHQC scheme under a slight global Rabi-frequency error due to the unwanted leakage to the ancillary system.

In this paper, we are motivated to propose a scheme for nonadiabatic holonomic multiqubit gates with two dark paths (NHMGTD) in the Rydberg atoms. In contrast to the NHQCTD schemes in the trapped-ion systems [70, 71], our scheme is free of the ancillary system. In particular, we can focus on an effective four-level configuration in the multiple Rydberg atomic system through tuning the driving fields on both control and target atoms. The time evolution operator $U(\tau)$ for the four-level configuration can be obtained by the dark-path method rather than the time-ordered integral of the effective Hamiltonian in the NHQC scheme. In our scheme, one dark path is provided by the dark state

* Email address: jingjun@zju.edu.cn

of the system Hamiltonian with zero eigenvalue, which is decoupled from the dynamical process. And another one is obtained by the time-dependent Schrödinger equation with a vanishing expectation value about the effective Hamiltonian. The dark-path states and the other two states out of the computational space constitute a complete space for the effective evolution of the system. In the presence of the external decoherence, our scheme is superior to both the standard NHQC scheme and the NHQCTD schemes [70, 71] in the whole range of both global and local errors in Rabi frequency. Moreover, for the large-scale quantum computation, our scheme can be extended to the N -qubit controlled gates.

The rest of the paper is structured as follows. In Sec. II, we derive the effective Hamiltonian in a double Rydberg atomic system, which is used to construct a universal set of nonadiabatic holonomic two-qubit controlled gates with the dark paths of our NHMGTD scheme. We test the robustness of both control-NOT (CNOT) and control-Z (CZ) gates against the systematic error and the external decoherence. In Sec. III, we provide the effective Hamiltonian for the three-qubit controlled gates and demonstrate the robustness of the control-control-NOT (CCNOT) gate. In Sec. IV, we extend our scheme to the situation of N -qubit controlled gates. We conclude the whole paper in Sec. V.

II. NONADIABATIC HOLONOMIC TWO-QUBIT CONTROLLED GATES

A. Gate construction with dark paths

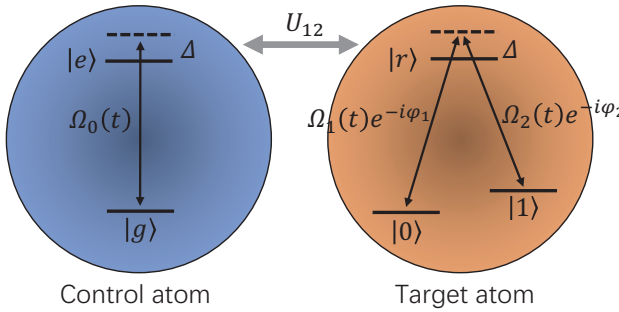


FIG. 1. Sketch of two coupled Rydberg atoms under driving. The control atom consists of the ground state $|g\rangle$ and the Rydberg state $|e\rangle$. The target atom consists of two ground states $|0\rangle$ and $|1\rangle$, and one Rydberg state $|r\rangle$. U_{12} is the van der Waals interaction between the Rydberg states of atoms.

Consider two coupled Rydberg atoms under driving by three laser fields as shown in Fig. 1. The control atom consists of the ground state $|g\rangle$ and the Rydberg state $|e\rangle$. The target atom has two stable low-energy states $|0\rangle$ and $|1\rangle$ and one Rydberg state $|r\rangle$. The control atom is driven by an off-resonant laser with the detuning Δ and the time-dependent Rabi frequency $\Omega_0(t)$. In the target

atom, the transitions $|0\rangle \leftrightarrow |r\rangle$ and $|1\rangle \leftrightarrow |r\rangle$ are driven respectively by the laser fields $\Omega_1(t)$ and $\Omega_2(t)$ with the same detuning Δ . φ_1 and φ_2 are two time-independent initial phases.

In the interaction picture with respect to the free Hamiltonian of the two atoms, the full Hamiltonian can be written as ($\hbar \equiv 1$)

$$H(t) = H_c(t) \otimes \mathcal{I}_t + \mathcal{I}_c \otimes H_t(t) + U_{12}|er\rangle\langle er|, \quad (1)$$

with

$$\begin{aligned} H_c(t) &= \Omega_0(t)e^{-i\Delta t}|e\rangle\langle g| + \text{H.c.}, \\ H_t(t) &= \Omega_1(t)e^{-i(\Delta t+\varphi_1)}|r\rangle_t\langle 0| \\ &+ \Omega_2(t)e^{-i(\Delta t+\varphi_2)}|r\rangle_t\langle 1| + \text{H.c.}, \end{aligned} \quad (2)$$

where \mathcal{I}_c and \mathcal{I}_t represent the identity operators in the space of control and target atoms, respectively. The interaction strength U_{12} between the high-lying Rydberg states can be obtained as $U_{12} = C_6/d_{12}^6$ [73, 74], where $C_6/2\pi \approx 1 \times 10^5$ GHz μm^6 is the coefficient of van der Waals interaction and d_{12} is the distance between Rydberg atoms lower-bounded by the diffraction limit.

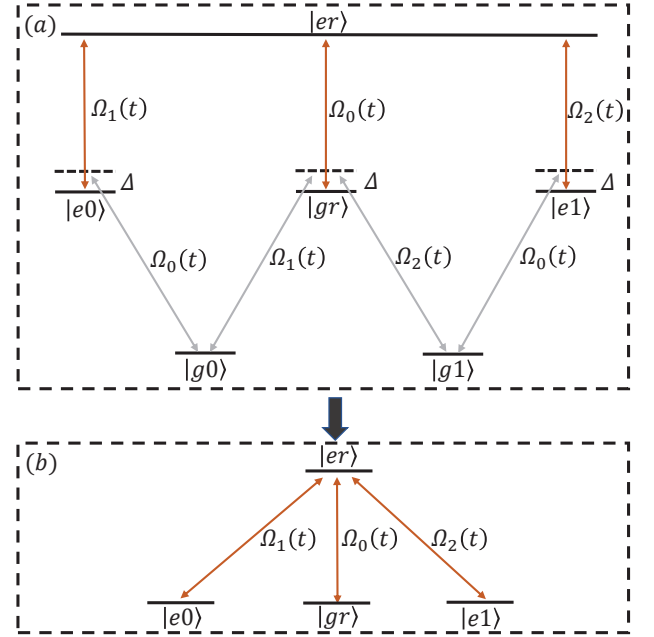


FIG. 2. (a) Transition diagram for the double Rydberg atomic system. The transitions plotted with the gray solid lines can be strongly suppressed under the condition of $U_{12} = \Delta \gg \Omega_0(t), \Omega_1(t), \Omega_2(t)$. (b) Effective four level configuration for the double Rydberg atomic system.

In the rotating frame with respect to $\mathcal{U}(t) = \exp(-iU_{12}t|er\rangle\langle er|)$, the Hamiltonian $H(t)$ in Eq. (1) can

be transformed to

$$\begin{aligned}
H_{\text{rot}}(t) &= \Omega_0(t)e^{-i\Delta t}(|e0\rangle\langle g0| + |e1\rangle\langle g1| + e^{iU_{12}t}|er\rangle\langle gr|) \\
&+ \Omega_1(t)e^{-i(\Delta t+\varphi_1)}(|gr\rangle\langle g0| + e^{iU_{12}t}|er\rangle\langle e0|) \\
&+ \Omega_2(t)e^{-i(\Delta t+\varphi_2)}(|gr\rangle\langle g1| + e^{iU_{12}t}|er\rangle\langle e1|) \\
&+ \text{H.c.},
\end{aligned} \tag{3}$$

as shown by the transition diagram in Fig. 2(a). Under the far-off-detuning condition that $U_{12} = \Delta \gg \Omega_0(t), \Omega_1(t), \Omega_2(t)$, a number of transitions [see the gray solid lines in Fig. 2(a)] are strongly suppressed. Then the Hamiltonian in Eq. (3) can be effectively expressed by a four-level configuration

$$\begin{aligned}
H_{\text{eff}}(t) &= \Omega_0(t)|er\rangle\langle gr| + \Omega_1(t)e^{-i\varphi_1}|er\rangle\langle e0| \\
&+ \Omega_2(t)e^{-i\varphi_2}|er\rangle\langle e1| + \text{H.c.},
\end{aligned} \tag{4}$$

as shown in Fig. 2(b). This effective Hamiltonian is verified by Fig. 10 in Appendix A. When the laser field on the control atom is turned off, i.e., $\Omega_0(t) = 0$, Fig. 2(b) reduces exactly to the Λ -level configuration for the standard NHQC scheme [55].

To construct the nonadiabatic holonomic two-qubit controlled gates with dark paths, the driving fields on the target atom can be parametrized by $\Omega_1(t) = \Omega(t)\sin\theta/2$ and $\Omega_2(t) = -\Omega(t)\cos\theta/2$, where $\Omega(t)$ and θ are time-dependent and time-independent, respectively. With the Morris-Shore transformation [75], the effective Hamiltonian in Eq. (4) can be recast as

$$H_{\text{eff}}(t) = \Omega(t)e^{i\varphi_2}|b\rangle\langle er| + \Omega_0(t)|gr\rangle\langle er| + \text{H.c.} \tag{5}$$

in the dark-bright basis with

$$\begin{aligned}
|b\rangle &= \sin\frac{\theta}{2}e^{i\varphi}|e0\rangle - \cos\frac{\theta}{2}|e1\rangle, \\
|D_1\rangle &= \cos\frac{\theta}{2}|e0\rangle + \sin\frac{\theta}{2}e^{-i\varphi}|e1\rangle,
\end{aligned} \tag{6}$$

where $\varphi \equiv \varphi_1 - \varphi_2$ and $|D_1\rangle$ is the dark state of $H_{\text{eff}}(t)$ with zero eigenvalue. $|D_1\rangle$ remains invariant during the evolution process for invariant θ and φ and forms the first dark path in our scheme.

The second dark path $|D_2\rangle = |D_2(t)\rangle$ is generally time dependent in our scheme, which can be defined by two constraints: (i) $|D_2\rangle$ is always orthogonal to $|D_1\rangle$, i.e., $\langle D_1|D_2\rangle = 0$; and (ii) the expectation value $\langle D_2|H_{\text{eff}}(t)|D_2\rangle$ remains vanishing during the gate construction, which accumulates no dynamical phase. Accordingly, $|D_2\rangle$ can be expressed by the following ansatz:

$$\begin{aligned}
|D_2\rangle &= \cos u(t)\cos v(t)e^{i\varphi_2}|b\rangle - i\sin u(t)|er\rangle \\
&- \cos u(t)\sin v(t)|gr\rangle
\end{aligned} \tag{7}$$

with two time-dependent parameters $u(t)$ and $v(t)$. By the Schrödinger equation $H_{\text{eff}}(t)|D_2(t)\rangle = id|D_2(t)\rangle/dt$,

the time-dependent Rabi frequencies $\Omega(t)$ and $\Omega_0(t)$ can be inversely determined by

$$\begin{aligned}
\Omega(t) &= \dot{v}(t)\cot u(t)\sin v(t) + \dot{u}(t)\cos v(t), \\
\Omega_0(t) &= \dot{v}(t)\cot u(t)\cos v(t) - \dot{u}(t)\sin v(t).
\end{aligned} \tag{8}$$

Under the cyclic condition for the gate construction lasting a period of τ , i.e., $\{|D_1\rangle, |D_2(\tau)\rangle\} = \{|e0\rangle, |e1\rangle\}$, the boundary conditions of $u(t)$ and $v(t)$ have to be $u(\tau) = u(0) = v(\tau) = v(0) = 0$. We follow Refs. [70, 71] and choose

$$u(t) = \frac{\pi}{2}\sin^2\left(\frac{\pi t}{\tau}\right), \quad v(t) = \eta[1 - \cos u(t)] \tag{9}$$

to ensure the cyclic evolution. By Eqs. (8) and (9), the tunable parameter η indicates both the driving laser applied on the control atom and the transition between the levels $|er\rangle$ and $|gr\rangle$ in Fig. 2(b). Specifically, a vanishing η corresponds to $v(t) = 0$ in Eq. (9), and it leads to $\Omega(t) \neq 0$ and $\Omega_0(t) = 0$ in Eq. (8), which describes the standard NHQC scheme [58] while a nonzero η representing our NHMGT scheme.

To implement a universal set of nonadiabatic holonomic two-qubit controlled gates, we adopt the multi-pulse single-loop method [58], in which the loop for gate construction is divided into two segments with equal intervals by adjusting the laser parameters. Accordingly, the cyclic evolution is completed by concatenating two unitary operators in the effective subspace:

$$\begin{aligned}
U(\tau/2, 0) &= |D_1\rangle\langle D_1| + |D_2(\tau/2)\rangle\langle D_2(0)| \\
&= |D_1\rangle\langle D_1| - i|er\rangle\langle b|, \\
U(\tau, \tau/2) &= |D_1\rangle\langle D_1| + |D_2(\tau)\rangle\langle D_2(\tau/2)| \\
&= |D_1\rangle\langle D_1| + ie^{i\gamma}|b\rangle\langle er|,
\end{aligned} \tag{10}$$

where the phase shift γ appears to be φ_2 in the second path segment. Consequently, the whole holonomic matrix of the whole geometric evolution is given by

$$U(\tau, 0) = |D_1\rangle\langle D_1| + e^{i\gamma}|b\rangle\langle b|. \tag{11}$$

In the gate space spanned by $\{|e0\rangle, |e1\rangle\}$, the holonomic matrix can be rewritten as

$$U(\theta, \varphi, \gamma) = U(\tau, 0) = |e\rangle\langle e| \otimes e^{i\frac{\gamma}{2}}e^{-i\frac{\gamma}{2}\vec{n}\cdot\vec{\sigma}}, \tag{12}$$

where $\vec{n} \equiv (\sin\theta\cos\varphi, \sin\theta\sin\varphi, \cos\theta)$, $\vec{\sigma}$ is the Pauli matrix, and $\exp(i\gamma/2)$ is a global phase factor. The unitary matrix $U(\theta, \varphi, \gamma)$ in Eq. (12) allows that the target atom can rotate about the desired axis \vec{n} by an arbitrary angle γ , provided that the control atom is prepared at the high-lying Rydberg state $|e\rangle$. The parameters θ , φ , and γ can be controlled by the Rabi frequencies and phases of the driving lasers. $U(\theta, \varphi, \gamma)$ therefore constructs an arbitrary nonadiabatic holonomic two-qubit controlled gate.

B. Gate performance

The performance of any quantum gates should be practically measured by the gate fidelity under both external

noises and systematic errors. The former could be described by the master equation [76] for the interested system, which reads,

$$\begin{aligned} \frac{\partial \rho}{\partial t} = & -i[H(t), \rho] + \frac{\kappa}{2}\mathcal{L}(\sigma_c^-) + \frac{\kappa_z}{2}\mathcal{L}(\sigma_c^z) \\ & + \frac{\kappa_0}{2}\mathcal{L}(|0\rangle_t\langle r|) + \frac{\kappa_1}{2}\mathcal{L}(|1\rangle_t\langle r|) + \frac{\kappa_z}{2}\mathcal{L}(\sigma_t^z). \end{aligned} \quad (13)$$

Here ρ is the density matrix for the coupled Rydberg atoms, $H(t)$ is their full Hamiltonian in Eq. (1), and $\mathcal{L}(o)$ is the Lindblad superoperators defined as $\mathcal{L}(o) \equiv 2o\rho o^\dagger - o^\dagger o\rho - \rho o^\dagger o$ [77], where $o = \sigma_c^-, \sigma_c^z, |0\rangle_t\langle r|, |1\rangle_t\langle r|, \sigma_t^z$. The superscripts and subscripts of these operators indicate the type of the quantum channels and the atom under decoherence, respectively. For examples, $\sigma_c^- \equiv |g\rangle_c\langle e|$ represents the dissipation channel of the control atom with a decay rate κ , and $|0\rangle_t\langle r|$ and $|1\rangle_t\langle r|$ represent the spontaneous emissions of the target atom from the Rydberg state $|r\rangle$ to the ground states $|0\rangle$ and $|1\rangle$ with decay rates κ_0 and κ_1 , respectively. For simplicity, we assume $\kappa_0 = \kappa_1 = \kappa/2$. The dephasing processes of the control atom and the target atom are described respectively by $\sigma_c^z \equiv |g\rangle_c\langle g| - |e\rangle_c\langle e|$ and $\sigma_t^z \equiv |0\rangle_t\langle 0| + |1\rangle_t\langle 1| - |r\rangle_t\langle r|$ with the same rate κ_z . For Rydberg atoms [24, 78], a typical decoherence rate κ of the Rydberg state ranges from $2\pi \times 0.75$ kHz to $2\pi \times 2.48$ kHz when the surrounding temperature T is in the range of $0 \sim 300$ K. And κ_z is close to κ in the order of magnitude [79].

The systematic errors in Rabi frequencies (driving strengths) could be grouped into the global and the local types, representing respectively the deviation for the full system and that for the target atom. Practically, the Hamiltonian $H(t)$ in Eq. (13) becomes

$$H(t) = (1 + \epsilon)[H_c(t) + (1 + \alpha)H_t(t)] + U_{12}|er\rangle\langle er|, \quad (14)$$

where ϵ and α are the dimensionless coefficients for the global and local Rabi-frequency errors, respectively.

To evaluate the gate performance of our NHMGTD scheme, we adopt the average fidelity function defined in Refs. [16, 80]

$$F = \frac{1}{N} \sum_{n=1}^N \langle \psi_n(0) | U^\dagger \rho(\tau) U | \psi_n(0) \rangle, \quad (15)$$

where $\rho(\tau)$ is obtained from Eqs. (13) and (14), $U = U(\theta, \varphi, \gamma)$ is the ideal two-qubit controlled gate (holonomic transformation) given in Eq. (12), and $|\psi_n(0)\rangle = |\psi_c(0)\rangle \otimes |\psi_t(0)\rangle$ is the n th benchmark state for the two-qubit system. In numerical simulation, the initial states of the control atom $|\psi_c(0)\rangle$ and the target atom $|\psi_t(0)\rangle$ are sampled respectively from the state sets $\{|g\rangle, |e\rangle, (|g\rangle + |e\rangle)/\sqrt{2}, (|g\rangle - |e\rangle)/\sqrt{2}, (|g\rangle + i|e\rangle)/\sqrt{2}, (|g\rangle - i|e\rangle)/\sqrt{2}\}$ and $\{|0\rangle, |1\rangle, (|0\rangle + |1\rangle)/\sqrt{2}, (|0\rangle - |1\rangle)/\sqrt{2}, (|0\rangle + i|1\rangle)/\sqrt{2}, (|0\rangle - i|1\rangle)/\sqrt{2}\}$. Thus $N = 6^2 = 36$ states are used in testing the two-qubit controlled gates. The choice of the benchmark states does not have significant influences on the gate performance. The type of the

holonomic two-qubit controlled gate, i.e., the parameters θ, φ, γ , are determined by the amplitudes and phases of the driving fields. We here focus on the CNOT gate $U(\pi/2, 0, \pi)$ and the CZ gate $U(0, 0, \pi)$.

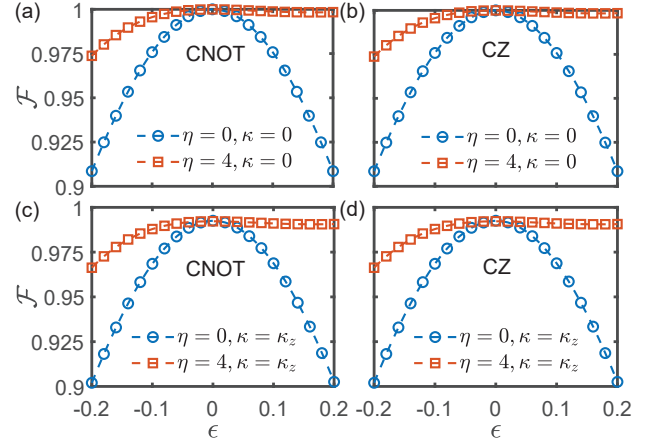


FIG. 3. Comparison about the average fidelity of our NHMGTD (with $\eta = 4$) and the existing NHQC (with $\eta = 0$) schemes under the global error ϵ in Rabi frequency of driving fields for (a) and (c) CNOT gates and (b) and (d) CZ gates in the absence (a) and (b) and in the presence (c) and (d) of dissipation. The detuning and the Rydberg-mediated interaction strength are $\Delta = U_{12} = 10^6 \kappa_z$, and in (c) and (d) the decay rate is set as $\kappa = \kappa_z$, where the dephasing rate is $\kappa_z = 2\pi \times 1$ kHz. The local error in Rabi frequency is set as $\alpha = 0$.

In Fig. 3, we compare our NHMGTD scheme and the standard NHQC scheme in the gate fidelities against the global error in Rabi frequency. As implied by Eq. (9), our scheme is distinct from the NHQC scheme by a non-vanishing η . Figure 3 demonstrates that in the presence or in the absence of the dissipation channels of the Rydberg atoms, the driving field on the control atom ($\eta = 4$) enhances significantly the gate robustness against the global Rabi-frequency error of the NHQC scheme ($\eta = 0$) for both CNOT and CZ gates in the whole range of $\epsilon \in [-0.2, 0.2]$. More interesting, it is found that the fidelity of our dark-path scheme is almost insensitive to a positive ϵ , which makes an asymmetric performance of our gates to $\epsilon = 0$. It is reasonable that a positive deviation means an enhanced driving laser that will reduce the running time of the holonomic gates.

In particular, for the CNOT gate with no dissipation in Fig. 3(a), its fidelity can be maintained above $F = 0.97$ with $\eta = 4$, higher than $F = 0.91$ with $\eta = 0$, even when the relative global error is as large as $\epsilon = -0.2$. For both CNOT and CZ gates [see Fig. 3(a) and Fig. 3(b)] with $\epsilon \geq 0$, our fidelity remains almost unit. Turning on the dissipation channel does not violate the advantage of our NHMGTD scheme over the NHQC scheme, although it decreases the fidelities for both CNOT and CZ gates. Note around the zero global error about the Rabi frequency, the previous dark-path scheme in the trapped-ion system [70, 71] has a poorer performance than the

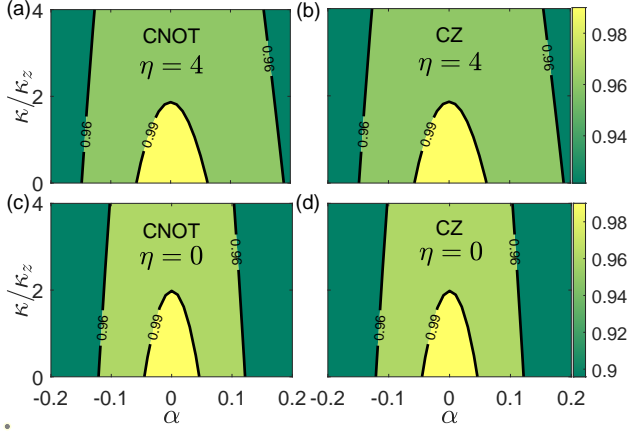


FIG. 4. Comparison about the fidelity landscape of our NHMGT [with $\eta = 4$ in (a) and (b)] and the NHQC [with $\eta = 0$ in (c) and (d)] schemes in the space of local error α in Rabi frequency of driving fields and decay rate κ for (a) and (c) CNOT gates and (b) and (d) CZ gates. The global Rabi frequency error is set as $\epsilon = 0$. The other parameters are set the same as those in Fig. 3.

standard NHQC scheme. In contrast, we can find that in both Fig. 3(c) and Fig. 3(d), the fidelity $F = 0.99$ with driving on the control atom $\eta = 4$ prevails $F = 0.98$ with no driving $\eta = 0$. It is due to the fact that our dark-path scheme in Rydberg atoms is conveniently controlled by an off-resonant laser field on the control atom instead of coupling the upper level of target atom to an ancillary system accompanied by an unwanted leakage.

Figure 4 demonstrates the fidelity landscape for both CNOT and CZ gates in the parameter space of local error coefficient α and decay rate κ , in which the dephasing channel indicated by $\kappa_z = 2\pi \times 1$ kHz is always on. The gate performance is distinguished by the regimes of $F \leq 0.96$ (see the dark green area), $0.96 \leq F \leq 0.99$ (see the light green area), and $F \geq 0.99$ (see the yellow area). Clearly the high-magnitude regimes in our NHMGT scheme ($\eta = 4$) are much broader than those in the NHQC scheme. In particular, when $\kappa = \kappa_z$, the CNOT-gate fidelity of our scheme can be maintained as $F = 0.99$ under the local Rabi-frequency error $\alpha = \pm 0.05$. In contrast, the same performance can survive up to $\alpha = \pm 0.03$ in the NHQC scheme. The off-resonant laser field on the control atom can thus improve the gate robustness in resisting the local Rabi frequency error.

III. NONADIABATIC HOLONOMIC THREE-QUBIT CONTROLLED GATES

A. Gate construction with dark paths

The three-qubit controlled gates are constructed with a system of three coupled Rydberg atoms. As shown in Fig. 5, again the control atoms and the target atom are respectively considered as two-level and three-level con-

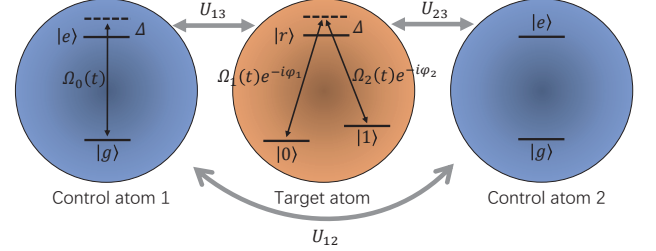


FIG. 5. Sketch of three coupled Rydberg atoms, where the first control atom and the target atom are under driving. U_{ij} ($i \neq j$) is the Rydberg-mediated interaction between the Rydberg states of atoms.

figurations. Note the second control atom is not under driving, which is merely coupled to the target atom and the first control atom via the Rydberg-mediated interactions U_{23} and U_{12} , respectively.

In the interaction picture with respect to the free Hamiltonian of the atoms, the full Hamiltonian reads

$$H(t) = H_{c_1}(t) + H_t(t) + H_I, \quad (16)$$

where

$$\begin{aligned} H_{c_1}(t) &= \Omega_0(t)e^{-i\Delta t}|e\rangle_{c_1}\langle g| + \text{H.c.}, \\ H_t(t) &= \Omega_1(t)e^{-i(\Delta t+\varphi_1)}|r\rangle_t\langle 0| \\ &\quad + \Omega_2(t)e^{-i(\Delta t+\varphi_2)}|r\rangle_t\langle 1| + \text{H.c.} \end{aligned} \quad (17)$$

are the driving Hamiltonians for the first control atom and the target atom, respectively, and

$$\begin{aligned} H_I &= U_{13}|e\rangle_{c_1}\langle e| \otimes \mathcal{I}_{c_2} \otimes |r\rangle_t\langle r| + U_{23}\mathcal{I}_{c_1} \otimes |er\rangle_{c_2}\langle er| \\ &\quad + U_{12}|ee\rangle_{c_1c_2}\langle ee| \otimes \mathcal{I}_t \end{aligned} \quad (18)$$

describes the interactions among the three atoms. This Hamiltonian could be realized in a Rydberg ion chain trapped in the optical lattice [29, 30], where the atom-atom interaction consists of the bare dipole-dipole interaction and the effective contribution induced by the electron-phonon coupling, i.e., $U_{ij} = V_{ij} + V_{ij}^{\text{eff}}$, $i \neq j$. V_{ij} and V_{ij}^{eff} depend on the atomic distance and the Rydberg potential gradient, respectively. Specifically, V_{ij}^{eff} can be conveniently tuned by the external laser fields [29, 30]. Due to the fact that a larger distance results in a weaker dipole-dipole interaction and a smaller gradient, the desired condition $U_{13} = U_{23} \gg U_{12}$ could be realized by the positions of these Rydberg ions $d_{13} = d_{23}$ and $d_{12} = 2d_{13}$.

In the rotating frame with respect to $\mathcal{U} = \exp(-iH_I)$, the Hamiltonian in Eq. (16) can be rewritten as

$$H_{\text{rot}}(t) = H'_{c_1}(t) + H'_t(t), \quad (19)$$

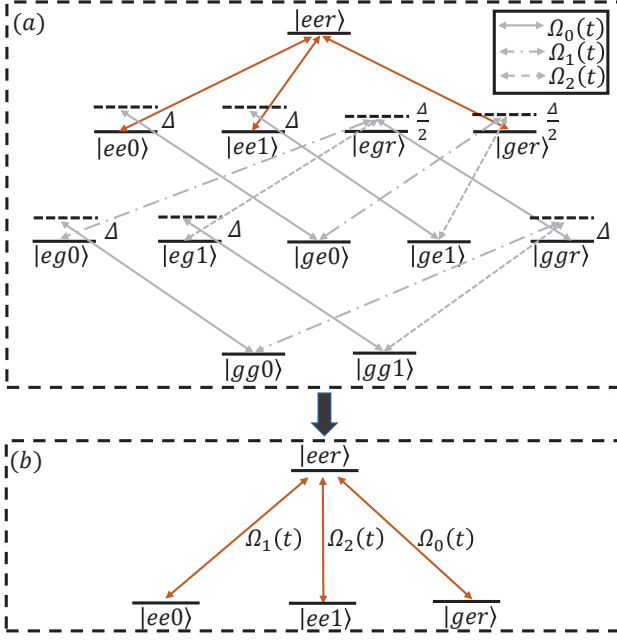


FIG. 6. (a) Transition diagram for the three Rydberg atomic system. The transitions plotted with the gray lines can be strongly suppressed under the condition of $U_{13} = U_{23} = (\Delta - U_{12})/2 \gg \Omega_0(t), \Omega_1(t), \Omega_2(t)$. (b) Effective four level configuration for the three Rydberg atomic system.

where

$$H'_{c1}(t) = \Omega_0(t)e^{-i\Delta t}(|eg0\rangle\langle gg0| + |eg1\rangle\langle gg1| + e^{iU_{13}t}|egr\rangle\langle ggr| + e^{iU_{12}t}|ee0\rangle\langle ee0| + e^{iU_{12}t}|ee1\rangle\langle ee1| + e^{i(U_{12}+U_{13}+U_{23})t}|eer\rangle\langle ger|) + \text{H.c.}, \quad (20)$$

and

$$H'_t(t) = \Omega_1(t)e^{-i(\Delta t+\varphi_1)}(|ggr\rangle\langle gg0| + e^{iU_{23}t}|ger\rangle\langle ge0| + e^{iU_{13}t}|egr\rangle\langle eg0| + e^{i(U_{12}+U_{13}+U_{23})t}|eer\rangle\langle ee0|) + \Omega_2(t)e^{-i(\Delta t+\varphi_2)}(|ggr\rangle\langle gg1| + e^{iU_{23}t}|ger\rangle\langle ge1| + e^{iU_{13}t}|egr\rangle\langle eg1| + e^{i(U_{12}+U_{13}+U_{23})t}|eer\rangle\langle ee1|) + \text{H.c.}, \quad (21)$$

as shown by the transition diagram in Fig. 6(a). Under the far-off-detuning condition that $U_{13} = U_{23} = (\Delta - U_{12})/2 \gg \Omega_0(t), \Omega_1(t), \Omega_2(t)$, a number of transitions [see the gray lines in Fig. 6(a)] are strongly suppressed. In particular, the gray solid lines represent the off-resonant terms with Rabi frequency $\Omega_0(t)$ in $H'_{c1}(t)$, and the gray dashed lines and gray dot-dashed lines represent respectively the off-resonant terms with Rabi frequencies $\Omega_1(t)$ and $\Omega_2(t)$ in $H'_t(t)$. The survival transitions constitute an effective Hamiltonian with a four-level

configuration

$$H_{\text{eff}}(t) = \Omega_0(t)|eer\rangle\langle ger| + \Omega_1(t)e^{-i\varphi_1}|eer\rangle\langle ee0| + \Omega_2(t)e^{-i\varphi_2}|eer\rangle\langle ee1| + \text{H.c.}, \quad (22)$$

as shown in Fig. 6(b). In Fig. 11 of Appendix A, we verify this effective Hamiltonian and estimate the influence from a weak Rydberg-mediated interaction U_{12} . Similar to the double atomic system, Fig. 6(b) reduces exactly to the standard NHQC scheme when the driving laser on the first control atom is turned off.

Using the same parametric setting in Eq. (5) and the Morris-Shore transformation, the effective Hamiltonian in Eq. (22) can be written as

$$H_{\text{eff}}(t) = \Omega(t)e^{i\varphi_2}|b\rangle\langle eer| + \Omega_0(t)|ger\rangle\langle eer| + \text{H.c.}, \quad (23)$$

where the bright state and the first dark path are

$$|b\rangle = \sin \frac{\theta}{2} e^{i\varphi} |ee0\rangle - \cos \frac{\theta}{2} |ee1\rangle, \quad (24)$$

$$|D_1\rangle = \cos \frac{\theta}{2} |ee0\rangle + \sin \frac{\theta}{2} e^{-i\varphi} |ee1\rangle,$$

respectively. Under the similar constraints as those in the double-qubit-gate case, the ansatz of the second dark path can be given by

$$|D_2(t)\rangle = \cos u(t) \cos v(t) e^{i\varphi_2} |b\rangle - i \sin u(t) |eer\rangle, \quad (25)$$

$$- \cos u(t) \sin v(t) |ger\rangle,$$

where the two time-dependent parameters $u(t)$ and $v(t)$ could also be chosen as in Eq. (9) due to the boundary condition. And the time-dependent parameters $\Omega(t)$ and $\Omega_0(t)$ still follow the same relation given by Eq. (8) with $u(t)$ and $v(t)$.

The multipulse single-loop method [58] is again adopted to construct a universal set of nonadiabatic holonomic three-qubit controlled gates, by which the cyclic evolution loop $U(\tau, 0)$ is a product of

$$U\left(\frac{\tau}{2}, 0\right) = |D_1\rangle\langle D_1| - i|eer\rangle\langle b|, \quad (26)$$

$$U\left(\tau, \frac{\tau}{2}\right) = |D_1\rangle\langle D_1| + ie^{i\gamma}|b\rangle\langle eer|,$$

resulting in the same form of Eq. (11). In the gate space spanned by $\{|ee0\rangle, |ee1\rangle\}$, the unitary matrix for an arbitrary nonadiabatic holonomic three-qubit controlled gate can be written as

$$U(\theta, \varphi, \gamma) = U(\tau, 0) = |ee\rangle\langle ee| \otimes e^{i\frac{\gamma}{2}} e^{-i\frac{\gamma}{2}\vec{n}\cdot\vec{\sigma}}. \quad (27)$$

The target atom can therefore rotate around the desired axis \vec{n} by a desired angle γ as long as both control atoms are simultaneously at the high-lying Rydberg state. We here focus on the control-control-NOT gate by choosing $\theta = \pi/2$, $\varphi = 0$, and $\gamma = \pi$.

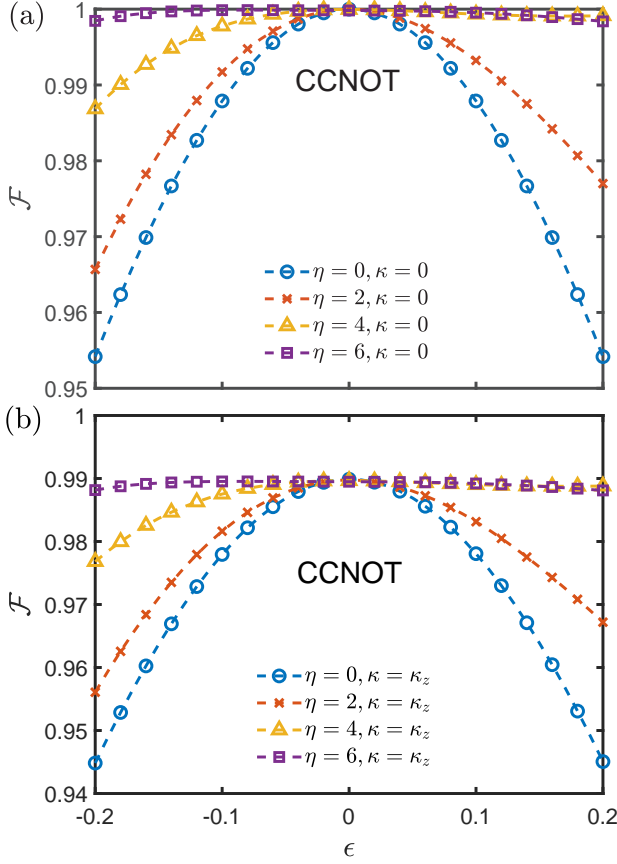


FIG. 7. Comparisons about the CCNOT-gate fidelity for NMGTD (with various nonvanishing η) and NHQC (with $\eta = 0$) schemes under the global error ϵ in Rabi frequency of the driving fields. (a) and (b) represent respectively the cases of $\kappa = 0$ (dissipation-free) and $\kappa = \kappa_z$. $\Delta/2 = U_{13} = U_{23} = 5 \times 10^5 \kappa_z$, $U_{12} = 0$, and $\kappa_z = 2\pi \times 1$ kHz. The local error coefficient is set as $\alpha = 0$.

B. Gate performance

Taking account the second control atom into consideration, the master equation (13) becomes

$$\begin{aligned} \frac{\partial \rho}{\partial t} = & -i[H(t), \rho] + \sum_{i=1}^2 \left[\frac{\kappa}{2} \mathcal{L}(\sigma_{c_i}^-) + \frac{\kappa_z}{2} \mathcal{L}(\sigma_{c_i}^z) \right] \\ & + \frac{\kappa}{4} \mathcal{L}(|0\rangle_t \langle r|) + \frac{\kappa}{4} \mathcal{L}(|1\rangle_t \langle r|) + \frac{\kappa_z}{2} \mathcal{L}(\sigma_t^z), \end{aligned} \quad (28)$$

where $H(t)$ is the full Hamiltonian of three coupled Rydberg atoms in Eq. (16), and $\sigma_{c_i}^-$ and $\sigma_{c_i}^z$ describe the dissipation and dephasing processes of the i th control atom, respectively.

Considering the systematic errors associated with the driving strengths (Rabi frequencies), the Hamiltonian in Eq. (16) can become

$$H(t) = (1 + \epsilon)[H_{c_1}(t) + (1 + \alpha)H_t(t)] + H_I, \quad (29)$$

where ϵ and α represent again the dimensionless coefficients for the global and local errors, respectively.

We formally use the average fidelity defined in Eq. (15) to evaluate the performance of our NMGTD scheme in constructing the three-qubit gates, where the benchmark states $|\psi_n(0)\rangle = |\psi_{c_1}\rangle \otimes |\psi_{c_2}\rangle \otimes |\psi_t\rangle$ are chosen respectively from the set of $\{|g\rangle, |e\rangle, (|g\rangle + |e\rangle)/\sqrt{2}, (|g\rangle - |e\rangle)/\sqrt{2}\}$, which is for the control atoms, and that of $\{|0\rangle, |1\rangle, (|0\rangle + |1\rangle)/\sqrt{2}, (|0\rangle - |1\rangle)/\sqrt{2}\}$, which is for the target atom. $N = 4^3 = 64$ states are therefore used in the simulation. In numerical evaluation, $U_{12} = 0$ is assumed for simplicity. It is found in Fig. 11 that the gate performance is hardly affected even when $U_{12} = U_{13}/5$.

In Fig. 7, we compare our scheme and the standard NHQC scheme in the CCNOT gate fidelities under the global error in Rabi frequency. In the absence [see Fig. 7(a)] and in the presence [see Fig. 7(b)] of the quantum dissipation, it is demonstrated that our NMGTD scheme prevails the NHQC scheme. It is deterministic to find that enhancing the driving field on the first control atom can improve significantly the capacity of our CCNOT gate in resisting the global Rabi-frequency error in the whole range of $\epsilon \in [-0.2, 0.2]$. In particular, for the dissipation-free CCNOT gate in Fig. 7(a), the fidelities of our scheme can be maintained as high as $F \approx 0.97$, $F \approx 0.99$, and almost unit respectively by $\eta = 2$, $\eta = 4$, and $\eta = 6$, even when $\epsilon = -0.2$. In contrast, the fidelity of NHQC scheme is less than 0.96. Note a high-fidelity gate still favors a positive instead of a negative ϵ . In the presence of dissipation in Fig. 7(b), all the preceding fidelities of the CCNOT gate will accordingly drop about one percentage.

In addition, we find that the CCNOT gate has a better performance than the CNOT gate by comparing Fig. 7(a) to Fig. 3(a) or by comparing Fig. 7(b) to Fig. 3(c). Under the same driving of $\eta = 4$ and when $\epsilon = -0.2$, the fidelity of the CCNOT gate is higher than that of the CNOT gate by almost one percentage. It indicates that the three-qubit holonomic gate of our scheme is less susceptible to the global error in Rabi frequency than the double-qubit gate.

The response of our CCNOT gate to the local error in the Rabi frequency can be reflected on the comparison about the landscape of Fig. 8(a) for our NMGTD scheme and that of Fig. 8(b) for the standard NHQC scheme. It is found that the high-fidelity regions by our NMGTD scheme are much broader than those by the NHQC scheme. In particular, when $\kappa = 0.5\kappa_z$, we have $F \geq 0.99$ in the range of $\alpha = [-0.05, 0.05]$ in Fig. 8(a). In contrast, when $\kappa = 0.5\kappa_z$, the fidelity could be maintained about $F \geq 0.99$ in the range of $\alpha = [-0.04, 0.04]$ in Fig. 8(b).

Additionally, by contrasting Fig. 8(a) to Fig. 4(a), one can find that the CCNOT gate is more resistant to the local Rabi frequency error α than the CNOT gate, yet it is more susceptible to the environmental dissipation $\kappa \neq 0$ in the presence of a small α . In particular, the bright yellow region for $F \geq 0.99$ in Fig. 8(a) is much broader than that in Fig. 4(a). And the upper-bound of κ/κ_z around $\alpha \approx 0$ for $F \geq 0.99$ is nearly 2.0 in Fig. 4(a), which is

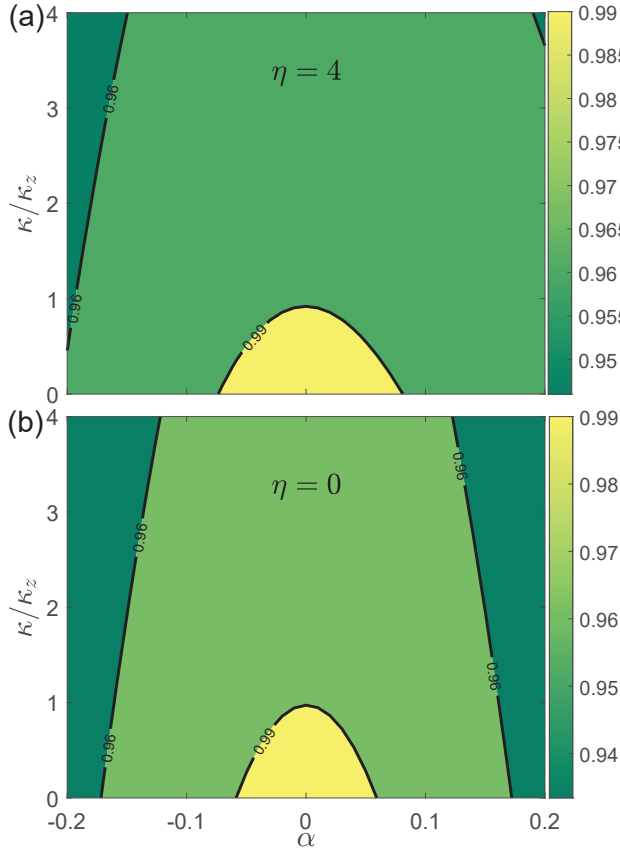


FIG. 8. Comparisons about the CCNOT-gate fidelity landscape for NHMGTD [with $\eta = 4$ in (a)] and NHQD [with $\eta = 0$ in (b)] schemes in the space of local error α in Rabi frequency of driving fields and decay rate κ . The global Rabi frequency error is set as $\epsilon = 0$. The other parameters are set the same as Fig. 7.

about two times of that in Fig. 8(a). Thus the advantage of the three-qubit holonomic gate of our scheme distinguishes in the absence of the environmental decoherence.

IV. NONADIABATIC HOLONOMIC N -QUBIT CONTROLLED GATES

To generalize our NHMGTD scheme to the N -qubit case, we can consider a multiple Rydberg atomic model as shown in Fig. 9. This model can be regarded as a direct extension of the three-atomic one in Fig. 5. Still only the first control atom and the target atom are under driving. And all the control atoms (in a two-level configuration) are coupled to the central target atom (in a three-level configuration) via the same coupling strength V . The interactions among the control atoms are omitted for simplicity.

In the interaction picture with respect to the free Hamiltonian of all these Rydberg atoms, the full Hamiltonian of the system have the same formation as Eq. (16):

$$H(t) = H_{c_1}(t) + H_t(t) + H_I, \quad (30)$$

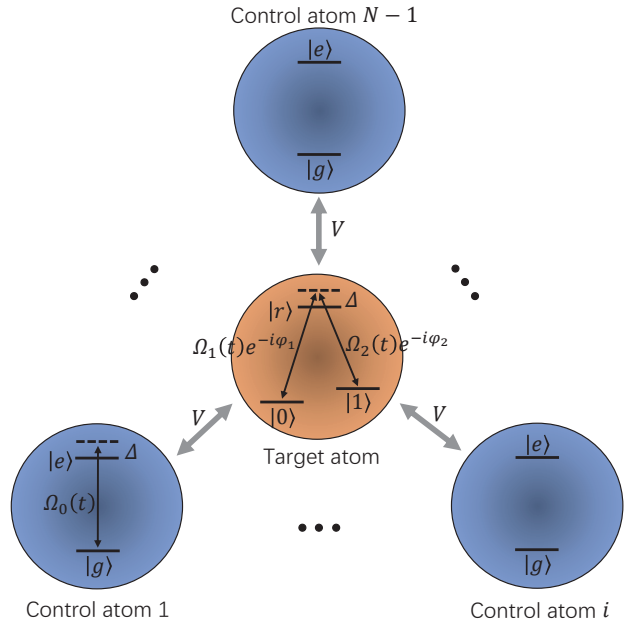


FIG. 9. Sketch of multiple coupled Rydberg atoms, where only the first control atom and the target atom are under driving. V represents the homogenous Rydberg-mediated interaction between the control atoms and the target atom.

where

$$\begin{aligned} H_{c_1}(t) &= \Omega_0(t)e^{-i\Delta t}|e\rangle_{c_1}\langle g| + \text{H.c.}, \\ H_t(t) &= \Omega_1(t)e^{-i(\Delta t+\varphi_1)}|r\rangle_t\langle 0| \\ &+ \Omega_2(t)e^{-i(\Delta t+\varphi_2)}|r\rangle_t\langle 1| + \text{H.c.}, \end{aligned} \quad (31)$$

$$H_I = V \sum_{i=1}^{N-1} |er\rangle_{c_i t} \langle er|.$$

Note the term $V|er\rangle_{c_i t} \langle er|$ in H_I represents the Rydberg-mediated interaction between the i th control atom and the target atom.

In the rotating frame with respect to $\mathcal{U} = \exp(-iH_I t)$, the Hamiltonian in Eq. (30) can be written as

$$H_{\text{rot}}(t) = H'_{c_1}(t) + H'_t(t), \quad (32)$$

where

$$\begin{aligned} H'_{c_1}(t) &= \Omega_0(t)e^{-i\Delta t}(|eg\cdots g0\rangle\langle gg\cdots g0| \\ &+ |eg\cdots g1\rangle\langle gg\cdots g1| + e^{iVt}|eg\cdots gr\rangle\langle gg\cdots gr| \\ &+ \cdots + |ee\cdots e0\rangle\langle ge\cdots e0| + |ee\cdots e1\rangle\langle ee\cdots e1| \\ &+ e^{i(N-1)Vt}|ee\cdots er\rangle\langle ge\cdots er|) + \text{H.c.}, \end{aligned} \quad (33)$$

and

$$\begin{aligned}
H'_t(t) = & \Omega_1(t)e^{-i(\Delta t+\varphi_1)}(|gg\cdots gr\rangle\langle gg\cdots g0| \\
& + e^{iVt}|gg\cdots er\rangle\langle gg\cdots e0| + \dots \\
& + e^{i(N-2)Vt}|ee\cdots gr\rangle\langle ee\cdots g0| \\
& + e^{i(N-1)Vt}|ee\cdots er\rangle\langle ee\cdots e0|) \\
& + \Omega_2(t)e^{-i(\Delta t+\varphi_2)}(|gg\cdots gr\rangle\langle gg\cdots g1| \\
& + e^{iVt}|gg\cdots er\rangle\langle gg\cdots e1| + \dots \\
& + e^{i(N-2)Vt}|ee\cdots gr\rangle\langle ee\cdots g1| \\
& + e^{i(N-1)Vt}|ee\cdots er\rangle\langle ee\cdots e1|) + \text{H.c.}
\end{aligned} \tag{34}$$

Under the far-off-detuning condition that $V = \Delta/(N-1) \gg \Omega_0(t), \Omega_1(t), \Omega_2(t)$, the Hamiltonian in Eq. (32) can be reduced to an effective four-level configuration as

$$\begin{aligned}
H_{\text{eff}}(t) = & \Omega_0(t)|ee\cdots er\rangle\langle ge\cdots er| \\
& + \Omega_1(t)e^{-i\varphi_1}|ee\cdots er\rangle\langle ee\cdots e0| \\
& + \Omega_2(t)e^{-i\varphi_2}|ee\cdots er\rangle\langle ee\cdots e1| + \text{H.c.},
\end{aligned} \tag{35}$$

which is demanded in constructing the N -qubit controlled gates with our scheme. Using the similar parametric settings in Eqs. (5) and (23) and the Morris-Shore transformation, the effective Hamiltonian in Eq. (35) can be recast to

$$\begin{aligned}
H_{\text{eff}}(t) = & \Omega(t)e^{i\varphi_2}|b\rangle\langle ee\cdots er| \\
& + \Omega_0(t)|ge\cdots er\rangle\langle ee\cdots er| + \text{H.c.}
\end{aligned} \tag{36}$$

with the bright and dark states

$$\begin{aligned}
|b\rangle = & \sin \frac{\theta}{2} e^{i\varphi} |ee\cdots e0\rangle - \cos \frac{\theta}{2} |ee\cdots e1\rangle, \\
|D_1\rangle = & \cos \frac{\theta}{2} |ee\cdots e0\rangle + \sin \frac{\theta}{2} e^{-i\varphi} |ee\cdots e1\rangle,
\end{aligned} \tag{37}$$

where the time-independent dark state $|D_1\rangle$ constitutes the first dark path. Similar to the preceding two- and three-qubit gates, the second dark path state can be constructed as

$$\begin{aligned}
|D_2(t)\rangle = & \cos u(t) \cos v(t) e^{i\varphi_2} |b\rangle - i \sin u(t) |ee\cdots er\rangle \\
& - \cos u(t) \sin v(t) |ge\cdots er\rangle,
\end{aligned} \tag{38}$$

with the same time-dependent setting about $u(t)$ and $v(t)$ as the coefficients in the two- and three-qubit controlled gates. And the time-dependant parameters $\Omega(t)$ and $\Omega_0(t)$ are determined by Eq. (8) as well.

Arbitrary holonomic N -qubit controlled gates can be implemented by using the multipulse single-loop technique [58], which results in the holonomic matrix of the same formation in Eq. (11). In the gate subspace $\{|ee\cdots e0\rangle, |ee\cdots e1\rangle\}$, the unitary transformation can be written as $U(\theta, \varphi, \gamma) = U(\tau, 0) = |ee\cdots e\rangle\langle ee\cdots e| \otimes e^{i\frac{\gamma}{2}} e^{-i\frac{\gamma}{2}\vec{n}\cdot\vec{\sigma}}$. It indicates that the rotation of the target atom can be launched when $N-1$ control atoms are prepared at the Rydberg state $|e\rangle$. Different multi-qubit

geometric gates can be realized through modulating the amplitudes and phases of driving fields, such as the C_N -NOT gate $U(\pi/2, 0, \pi)$ and the C_N -Z gate $U(0, 0, \pi)$. In general, $U(\theta, \varphi, \gamma)$ constructs an arbitrary nonadiabatic holonomic N -qubit controlled gate.

V. CONCLUSION

In summary, we have constructed arbitrary nonadiabatic holonomic N -qubit controlled gates based on the dark paths in the Rydberg atomic system. Through modulating the detuning of driving fields on the target atom and one of the control atoms to be near-resonant with the summation of the coupling strength between target atom and control atoms, the dynamics of the coupled Rydberg atomic system could be effectively described in a four-level configuration. Thereby the time-evolution operator for arbitrary geometric controlled gates in our NHMGTD scheme can be inversely engineered by two dark paths and the multipulse single-loop method. In contrast to the existing dark-path scheme [70, 71], our scheme avoids the leakage to the ancillary system and can be conveniently performed by the driving field on the control atom. Then our scheme could extend the advantage of the dark-path schemes over the standard NHQC scheme in resisting the systematic errors in Rabi-frequency from the closed-system scenario to the open-system one. By virtue of the high-performance in gate fidelity and the scalability to more qubits, our scheme is of interest in the pursuit of high-speed and large-scale quantum computation.

Appendix A: Effective Hamiltonian for double-qubit and three-qubit gates

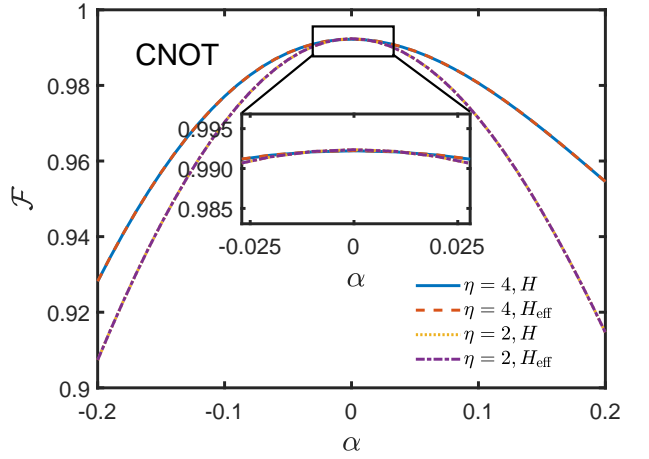


FIG. 10. Average fidelity of our CNOT gate under various parameter η of the driving on the control atom versus the local error in Rabi frequency. $\epsilon = 0$, $\kappa = \kappa_z$, and the other parameters are set the same as those in Fig. 4.

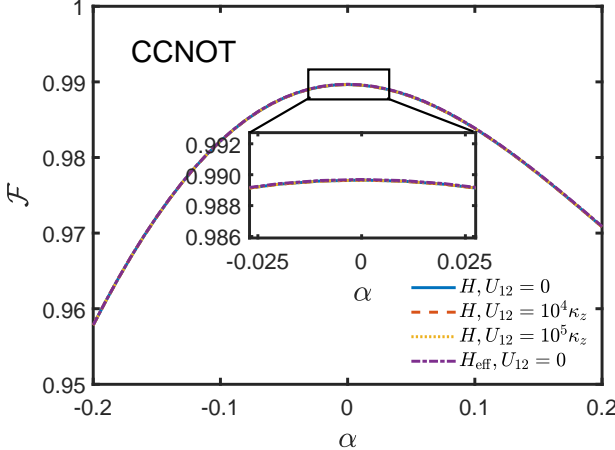


FIG. 11. Average fidelity of our CCNOT gate with $\eta = 4$ versus the local error in Rabi frequency. $\epsilon = 0$, $\kappa = \kappa_z$, and the other parameters are set the same as those in Fig. 8.

This appendix contributes to verifying the effective Hamiltonian in Eq. (4) for the two-qubit gate and that in Eq. (22) for the three-qubit gate through comparing the gate fidelities obtained by the full Hamiltonian and those obtained by the effective Hamiltonian. In the case of the three-qubit gate, we also estimate the influence from a nonvanishing Rydberg-mediated interaction U_{12} between the control atoms on the fidelity.

In Fig. 10, we show the fidelity of the CNOT gate under the local Rabi-frequency error. With $\eta = 2$ or $\eta = 4$, it is found that the results by the full Hamiltonian in Eq. (1) are coincident with those by the effective Hamiltonian in Eq. (4). It is interesting to see all the curves become indistinguishable around $\alpha = 0$.

As for the CCNOT gate, it is noted that in Figs. 7 and 8, the interaction between the controlled atoms U_{12} is assumed to be ignorable in comparison to those between the control atoms and the target atom U_{13} and U_{23} . We demonstrate in Fig. 11 that the results by the effective Hamiltonian under $U_{12} = 0$ are indeed indistinguishable from those by the full Hamiltonian with up to $U_{12} = 10^5 \kappa_z = U_{13}/5$. In another word, our scheme is insensitive to a weak interaction U_{12} . Then we can confirm the necessary condition for our scheme that the detuning of driving fields on the target atom and one of the control atoms to be near-resonant with the summation of the coupling strength between target atom and control atoms, i.e., $\Delta \approx (N-1)V$, where V is the same coupling strength between the control atoms and the target atom.

ACKNOWLEDGMENTS

We acknowledge financial support from the National Natural Science Foundation of China (Grant No. 11974311).

[1] P. W. Shor, *Polynomial-time algorithms for prime factorization and discrete logarithms on a quantum computer*, *SIAM J. Comput.* **26**, 1484 (1997).

[2] L. K. Grover, *Quantum mechanics helps in searching for a needle in a haystack*, *Phys. Rev. Lett.* **79**, 325 (1997).

[3] P. W. Shor, *Scheme for reducing decoherence in quantum computer memory*, *Phys. Rev. A* **52**, R2493 (1995).

[4] A. M. Steane, *Error correcting codes in quantum theory*, *Phys. Rev. Lett.* **77**, 793 (1996).

[5] L. K. Grover, *Quantum computers can search rapidly by using almost any transformation*, *Phys. Rev. Lett.* **80**, 4329 (1998).

[6] L. M. K. Vandersypen, M. Steffen, G. Breyta, C. S. Yannoni, M. H. Sherwood, and I. L. Chuang, *Experimental realization of shor's quantum factoring algorithm using nuclear magnetic resonance*, *Nature(London)* **414**, 883 (2001).

[7] A. Joshi and M. Xiao, *Three-qubit quantum-gate operation in a cavity qed system*, *Phys. Rev. A* **74**, 052318 (2006).

[8] W. L. Yang, C. Y. Chen, and M. Feng, *Implementation of three-qubit grover search in cavity quantum electrodynamics*, *Phys. Rev. A* **76**, 054301 (2007).

[9] A. Barenco, C. H. Bennett, R. Cleve, D. P. DiVincenzo, N. Margolus, P. Shor, T. Sleator, J. A. Smolin, and H. Weinfurter, *Elementary gates for quantum computation*, *Phys. Rev. A* **52**, 3457 (1995).

[10] E. Urban, T. A. Johnson, T. Henage, L. Isenhower, D. D. Yavuz, T. G. Walker, and M. Saffman, *Observation of rydberg blockade between two atoms*, *Nat. Phys.* **5**, 110 (2009).

[11] D. Møller, L. B. Madsen, and K. Mølmer, *Quantum gates and multiparticle entanglement by rydberg excitation blockade and adiabatic passage*, *Phys. Rev. Lett.* **100**, 170504 (2008).

[12] M. Saffman and K. Mølmer, *Efficient multiparticle entanglement via asymmetric rydberg blockade*, *Phys. Rev. Lett.* **102**, 240502 (2009).

[13] S.-B. Zheng, *Implementation of toffoli gates with a single asymmetric heisenberg xy interaction*, *Phys. Rev. A* **87**, 042318 (2013).

[14] C. Monroe, D. M. Meekhof, B. E. King, W. M. Itano, and D. J. Wineland, *Demonstration of a fundamental quantum logic gate*, *Phys. Rev. Lett.* **75**, 4714 (1995).

[15] F. Schmidt-Kaler, H. Häffner, M. Riebe, S. Gulde, G. P. T. Lancaster, T. Deuschle, C. Becher, C. F. Roos, J. Eschner, and R. Blatt, *Realization of the cirac-zoller controlled-not quantum gate*, *Nature(London)* **422**, 408 (2003).

[16] T. Monz, K. Kim, W. Hänsel, M. Riebe, A. S. Villar, P. Schindler, M. Chwalla, M. Hennrich, and R. Blatt, *Realization of the quantum toffoli gate with trapped ions*, *Phys. Rev. Lett.* **102**, 040501 (2009).

[17] T. Yamamoto, Y. A. Pashkin, O. Astafiev, Y. Nakamura, and J. S. Tsai, *Demonstration of conditional gate operation using superconducting charge qubits*, *Nature(London)* **425**, 941 (2003).

[18] J. H. Plantenberg, P. C. de Groot, C. J. P. M. Harmans, and J. E. Mooij, *Demonstration of controlled-not quantum gates on a pair of superconducting quantum bits*, *Nature(London)* **447**, 836 (2007).

[19] A. Fedorov, L. Steffen, M. Baur, M. P. da Silva, and A. Wallraff, *Implementation of a toffoli gate with superconducting circuits*, *Nature(London)* **481**, 170 (2012).

[20] J. L. O'Brien, G. J. Pryde, A. G. White, T. C. Ralph, and D. Branning, *Demonstration of an all-optical quantum controlled-not gate*, *Nature(London)* **426**, 264 (2003).

[21] T. B. Pittman, M. J. Fitch, B. C. Jacobs, and J. D. Franson, *Experimental controlled-not logic gate for single photons in the coincidence basis*, *Phys. Rev. A* **68**, 032316 (2003).

[22] M. Mičuda, M. Sedlák, I. Straka, M. Miková, M. Dušek, M. Ježek, and J. Fiurášek, *Efficient experimental estimation of fidelity of linear optical quantum toffoli gate*, *Phys. Rev. Lett.* **111**, 160407 (2013).

[23] T. M. Graham, M. Kwon, B. Grinkemeyer, Z. Marra, X. Jiang, M. T. Lichtman, Y. Sun, M. Ebert, and M. Saffman, *Rydberg-mediated entanglement in a two-dimensional neutral atom qubit array*, *Phys. Rev. Lett.* **123**, 230501 (2019).

[24] L. Isenhower, E. Urban, X. L. Zhang, A. T. Gill, T. Henage, T. A. Johnson, T. G. Walker, and M. Saffman, *Demonstration of a neutral atom controlled-not quantum gate*, *Phys. Rev. Lett.* **104**, 010503 (2010).

[25] H. Levine, A. Keesling, A. Omran, H. Bernien, S. Schwartz, A. S. Zibrov, M. Endres, M. Greiner, V. Vuletić, and M. D. Lukin, *High-fidelity control and entanglement of rydberg-atom qubits*, *Phys. Rev. Lett.* **121**, 123603 (2018).

[26] M. Saffman, T. G. Walker, and K. Mølmer, *Quantum information with rydberg atoms*, *Rev. Mod. Phys.* **82**, 2313 (2010).

[27] D. Jaksch, J. I. Cirac, P. Zoller, S. L. Rolston, R. Côté, and M. D. Lukin, *Fast quantum gates for neutral atoms*, *Phys. Rev. Lett.* **85**, 2208 (2000).

[28] D. Petrosyan, F. Motzoi, M. Saffman, and K. Mølmer, *High-fidelity rydberg quantum gate via a two-atom dark state*, *Phys. Rev. A* **96**, 042306 (2017).

[29] F. M. Gambetta, W. Li, F. Schmidt-Kaler, and I. Lesanovsky, *Engineering nonbinary rydberg interactions via phonons in an optical lattice*, *Phys. Rev. Lett.* **124**, 043402 (2020).

[30] F. M. Gambetta, C. Zhang, M. Hennrich, I. Lesanovsky, and W. Li, *Long-range multibody interactions and three-body antiblockade in a trapped rydberg ion chain*, *Phys. Rev. Lett.* **125**, 133602 (2020).

[31] J. T. Young, P. Bienias, R. Belyansky, A. M. Kaufman, and A. V. Gorshkov, *Asymmetric blockade and multiqubit gates via dipole-dipole interactions*, *Phys. Rev. Lett.* **127**, 120501 (2021).

[32] M. D. Lukin, M. Fleischhauer, R. Cote, L. M. Duan, D. Jaksch, J. I. Cirac, and P. Zoller, *Dipole blockade and quantum information processing in mesoscopic atomic ensembles*, *Phys. Rev. Lett.* **87**, 037901 (2001).

[33] M. Müller, I. Lesanovsky, H. Weimer, H. P. Büchler, and P. Zoller, *Mesoscopic rydberg gate based on electromagnetically induced transparency*, *Phys. Rev. Lett.* **102**, 170502 (2009).

[34] A. Gaëtan, Y. Miroshnychenko, T. Wilk, A. Chotia, M. Viteau, D. Comparat, P. Pillet, A. Browaeys, and P. Grangier, *Observation of collective excitation of two individual atoms in the rydberg blockade regime*, *Nat. Phys.* **5**, 115 (2009).

[35] C. Ates, T. Pohl, T. Pattard, and J. M. Rost, *Antiblockade in rydberg excitation of an ultracold lattice gas*, *Phys. Rev. Lett.* **98**, 023002 (2007).

[36] W. Li, C. Ates, and I. Lesanovsky, *Nonadiabatic motional effects and dissipative blockade for rydberg atoms excited from optical lattices or microtraps*, *Phys. Rev. Lett.* **110**, 213005 (2013).

[37] T. Pohl and P. R. Berman, *Breaking the dipole blockade: Nearly resonant dipole interactions in few-atom systems*, *Phys. Rev. Lett.* **102**, 013004 (2009).

[38] S.-L. Su, E. Liang, S. Zhang, J.-J. Wen, L.-L. Sun, Z. Jin, and A.-D. Zhu, *One-step implementation of the rydberg-rydberg-interaction gate*, *Phys. Rev. A* **93**, 012306 (2016).

[39] T. Wilk, A. Gaëtan, C. Evellin, J. Wolters, Y. Miroshnychenko, P. Grangier, and A. Browaeys, *Entanglement of two individual neutral atoms using rydberg blockade*, *Phys. Rev. Lett.* **104**, 010502 (2010).

[40] Y. Zeng, P. Xu, X. He, Y. Liu, M. Liu, J. Wang, D. J. Paupular, G. V. Shlyapnikov, and M. Zhan, *Entangling two individual atoms of different isotopes via rydberg blockade*, *Phys. Rev. Lett.* **119**, 160502 (2017).

[41] K. M. Maller, M. T. Lichtman, T. Xia, Y. Sun, M. J. Piotrowicz, A. W. Carr, L. Isenhower, and M. Saffman, *Rydberg-blockade controlled-not gate and entanglement in a two-dimensional array of neutral-atom qubits*, *Phys. Rev. A* **92**, 022336 (2015).

[42] C. J. Picken, R. Legaie, K. McDonnell, and J. D. Pritchard, *Entanglement of neutral-atom qubits with long ground-rydberg coherence times*, *Quantum Sci. Technol.* **4**, 015011 (2018).

[43] I. S. Madjarov, J. P. Covey, A. L. Shaw, J. Choi, A. Kale, A. Cooper, H. Pichler, V. Schkolnik, J. R. Williams, and M. Endres, *High-fidelity entanglement and detection of alkaline-earth rydberg atoms*, *Nat. Phys.* **5**, 115 (2009).

[44] P. Solinas, P. Zanardi, and N. Zanghì, *Robustness of non-abelian holonomic quantum gates against parametric noise*, *Phys. Rev. A* **70**, 042316 (2004).

[45] S.-L. Zhu and P. Zanardi, *Geometric quantum gates that are robust against stochastic control errors*, *Phys. Rev. A* **72**, 020301 (2005).

[46] P. Solinas, M. Sasetti, P. Truini, and N. Zanghì, *On the stability of quantum holonomic gates*, *New J. Phys.* **14**, 093006 (2012).

[47] M. Johansson, E. Sjöqvist, L. M. Andersson, M. Ericsson, B. Hessmo, K. Singh, and D. M. Tong, *Robustness of nonadiabatic holonomic gates*, *Phys. Rev. A* **86**, 062322 (2012).

[48] F. Wilczek and A. Zee, *Appearance of gauge structure in simple dynamical systems*, *Phys. Rev. Lett.* **52**, 2111 (1984).

[49] M. V. Berry, *Quantal phase factors accompanying adiabatic changes*, *Proc. R. Soc. Lond. A* **392**, 45 (1984).

[50] Y. Aharonov and J. Anandan, *Phase change during a cyclic quantum evolution*, *Phys. Rev. Lett.* **58**, 1593 (1987).

[51] J. Pachos, P. Zanardi, and M. Rasetti, *Non-abelian berry connections for quantum computation*, *Phys. Rev. A* **61**, 010305 (1999).

[52] L.-M. Duan, J. I. Cirac, and P. Zoller, *Geometric manipulation of trapped ions for quantum computation*,

Science **292**, 1695 (2001).

[53] L.-A. Wu, P. Zanardi, and D. A. Lidar, *Holonomic quantum computation in decoherence-free subspaces*, Phys. Rev. Lett. **95**, 130501 (2005).

[54] Y.-Y. Huang, Y.-K. Wu, F. Wang, P.-Y. Hou, W.-B. Wang, W.-G. Zhang, W.-Q. Lian, Y.-Q. Liu, H.-Y. Wang, H.-Y. Zhang, L. He, X.-Y. Chang, Y. Xu, and L.-M. Duan, *Experimental realization of robust geometric quantum gates with solid-state spins*, Phys. Rev. Lett. **122**, 010503 (2019).

[55] E. Sjöqvist, D. Tong, L. M. Andersson, B. Hessmo, M. Johansson, and K. Singh, *Non-adiabatic holonomic quantum computation*, New J. Phys. **14**, 103035 (2012).

[56] G. F. Xu, J. Zhang, D. M. Tong, E. Sjöqvist, and L. C. Kwek, *Nonadiabatic holonomic quantum computation in decoherence-free subspaces*, Phys. Rev. Lett. **109**, 170501 (2012).

[57] G. F. Xu, C. L. Liu, P. Z. Zhao, and D. M. Tong, *Nonadiabatic holonomic gates realized by a single-shot implementation*, Phys. Rev. A **92**, 052302 (2015).

[58] E. Herterich and E. Sjöqvist, *Single-loop multiple-pulse nonadiabatic holonomic quantum gates*, Phys. Rev. A **94**, 052310 (2016).

[59] G. T. Genov, D. Schraft, N. V. Vitanov, and T. Halfmann, *Arbitrarily accurate pulse sequences for robust dynamical decoupling*, Phys. Rev. Lett. **118**, 133202 (2017).

[60] P. Z. Zhao, X. Wu, and D. M. Tong, *Dynamical decoupling-protected nonadiabatic holonomic quantum computation*, Phys. Rev. A **103**, 012205 (2021).

[61] A. A. Abdumalikov Jr, J. M. Fink, K. Juliusson, M. Pechal, S. Berger, A. Wallraff, and S. Filipp, *Experimental realization of non-abelian non-adiabatic geometric gates*, Nature(London) **496**, 482 (2013).

[62] Y. Xu, W. Cai, Y. Ma, X. Mu, L. Hu, T. Chen, H. Wang, Y. P. Song, Z.-Y. Xue, Z.-q. Yin, and L. Sun, *Single-loop realization of arbitrary nonadiabatic holonomic single-qubit quantum gates in a superconducting circuit*, Phys. Rev. Lett. **121**, 110501 (2018).

[63] G. Feng, G. Xu, and G. Long, *Experimental realization of nonadiabatic holonomic quantum computation*, Phys. Rev. Lett. **110**, 190501 (2013).

[64] C. Zu, W.-B. Wang, L. He, W.-G. Zhang, C.-Y. Dai, F. Wang, and L.-M. Duan, *Experimental realization of universal geometric quantum gates with solid-state spins*, Nature(London) **514**, 72 (2014).

[65] Y. Sekiguchi, N. Niikura, R. Kuroiwa, H. Kano, and H. Kosaka, *Optical holonomic single quantum gates with a geometric spin under a zero field*, Nat. Photon. **11**, 309 (2017).

[66] S.-B. Zheng, C.-P. Yang, and F. Nori, *Comparison of the sensitivity to systematic errors between nonadiabatic non-abelian geometric gates and their dynamical counterparts*, Phys. Rev. A **93**, 032313 (2016).

[67] J. Jing, C.-H. Lam, and L.-A. Wu, *Non-abelian holonomic transformation in the presence of classical noise*, Phys. Rev. A **95**, 012334 (2017).

[68] A. Galindo and M. A. Martín-Delgado, *Information and computation: Classical and quantum aspects*, Rev. Mod. Phys. **74**, 347 (2002).

[69] D. Nigg, M. Müller, E. A. Martinez, P. Schindler, M. Hennrich, T. Monz, M. A. Martin-Delgado, and R. Blatt, *Quantum computations on a topologically encoded qubit*, Science **345**, 302 (2014).

[70] A. Ming-Zhong, L. Sai, H. Ran, X. Zheng-Yuan, C. Jin-Ming, H. Yun-Feng, L. Chuan-Feng, and G. Guang-Can, *Experimental realization of nonadiabatic holonomic single-qubit quantum gates with two dark paths in a trapped ion*, Fundam. Res. **2**, 661 (2022).

[71] T. André and E. Sjöqvist, *Dark path holonomic qudit computation*, Phys. Rev. A **106**, 062402 (2022).

[72] A. Baksic, H. Ribeiro, and A. A. Clerk, *Speeding up adiabatic quantum state transfer by using dressed states*, Phys. Rev. Lett. **116**, 230503 (2016).

[73] Y.-M. Liu, X.-D. Tian, D. Yan, Y. Zhang, C.-L. Cui, and J.-H. Wu, *Nonlinear modifications of photon correlations via controlled single and double rydberg blockade*, Phys. Rev. A **91**, 043802 (2015).

[74] D. Cano and J. Fortágh, *Multiatom entanglement in cold rydberg mixtures*, Phys. Rev. A **89**, 043413 (2014).

[75] J. R. Morris and B. W. Shore, *Reduction of degenerate two-level excitation to independent two-state systems*, Phys. Rev. A **27**, 906 (1983).

[76] H. Carmichael, *Statistical Methods in Quantum Optics* (Springer, Berlin, 1999).

[77] M. O. Scully and M. S. Zubairy, *Quantum Optics* (Cambridge University Press, Cambridge, 1997).

[78] I. I. Beterov, I. I. Ryabtsev, D. B. Tretyakov, and V. M. Entin, *Quasiclassical calculations of blackbody-radiation-induced depopulation rates and effective lifetimes of rydberg ns, np, and nd alkali-metal atoms with $n \leq 80$* , Phys. Rev. A **79**, 052504 (2009).

[79] L.-N. Sun, L.-L. Yan, S.-L. Su, and Y. Jia, *One-step implementation of time-optimal-control three-qubit nonadiabatic holonomic controlled gates in rydberg atoms*, Phys. Rev. Appl. **16**, 064040 (2021).

[80] Y. Liang, P. Shen, L.-N. Ji, and Z.-Y. Xue, *State-independent nonadiabatic geometric quantum gates*, Phys. Rev. Appl. **19**, 024051 (2023).